JOURNAL OF SOLID STATE CHEMISTRY 59, 201–209 (1985)

Electrical and Magnetic Properties and Homogeneity Ranges of Mixed-Valence Cesium–Vanadium Oxides

M. NYGREN, B. BLOM, AND B. FORSLUND

Department of Inorganic Chemistry, Arrhenius Laboratory, University of Stockholm, S-106 91 Stockholm, Sweden

AND M. WOŁCYRZ

Institute for Low Temperature and Structure Research, Polish Academy of Sciences, Pl. Katedralny 1, 50-950 Wrocław, Poland

Received October 5, 1984

Single crystals of CsV_2O_5, $Cs_2V_5O_{13}$, $Cs_xV_2O_5$, and CsV_3O_7, grown from melts, have been subjected to electrical conductivity and magnetic susceptibility measurements. CsV_2O_5 and $Cs_2V_5O_{13}$ are insulators exhibiting Curie–Weiss' law behavior with p_{eff} close to $1.73/V^{4+}$ ion. They are stoichiometric according to the X-ray studies. CsV_2O_5, which has a very limited composition range ($x \approx 0.30$–0.33), is a semiconductor with temperature-dependent paramagnetism ($p_{eff} = 1.83/V^{4+}$ ion). $Cs_xV_3O_7$ ($0.30 \lesssim x \lesssim 0.40$) is antiferromagnetic with a Néel temperature of ≈230 K. The temperature variation of the lattice parameters of $Cs_{0.33}V_3O_7$ has been determined with a Bond-type diffractometer. The same crystal was used for the conductivity measurements, and together these studies indicate that the transition from the semiconducting antiferromagnetic state to the semiconducting paramagnetic state takes place stepwise. The observed properties are discussed with reference to the crystal structures of the compounds.

Introduction

Systematic studies of electrical and magnetic properties of mixed-valence alkali vanadium oxides, frequently referred to as "vanadium oxide bronzes," have been undertaken since the early forties (*1, 2*). Comprehensive reports, in particular those concerning physical properties and crystal structure data of Li-, Na-, and K-vanadium oxide bronzes, have recently been published (see, e.g., Refs. (*3, 4*)).

Most physical measurements have so far been performed on polycrystalline samples. However, single crystals have been used in the studies of the electrical conductivity of β-$Na_xV_2O_5$ with $x \approx 0.3$. An unexpectedly large electrical anisotropy was thereby found and this compound has therefore been regarded as a quasi-one-dimensional metallic conductor (*5*).

Studies of subsolidus phase relations in the system Cs_2O–V_2O_5–VO_2 have shown that for $0 < Cs/V < 1$ four different mixed-valence Cs–V oxides exist, namely, $Cs_xV_3O_7$ ($x = 0.3$–0.4), $Cs_xV_2O_5$ ($x = 0.3$), $Cs_2V_5O_{13}$, and CsV_2O_5 (*6*). The crystal structures of these compounds had previously been determined (*7–10*). In subsequent studies of the phase relations at li-

0022-4596/85 $3.00

quidus temperatures it was demonstrated that single crystals could be grown from the melt in reducing atmospheres (*11, 12*).

Single crystals of the four Cs compounds have thus been used in this study of the electrical and magnetic properties. The lattice parameters of $Cs_{0.33}V_3O_7$ and their variation with temperature in the range 125–300 K have been accurately determined with the Bond method. The data obtained are discussed with special reference to the crystal structures.

Preparation

Powder samples of $Cs_xV_3O_7$ with $0.25 \leq x \leq 0.46$ and of compositions close to this line were prepared from appropriate amounts of $CsVO_3$, V_2O_5, and V_2O_3, thoroughly mixed and heated in evacuated silica tubes at 470°C for 14-day periods with intervening remixing. The temperature of preparation was chosen as high as possible below incipient melting (see Ref. (*11*)). Powder samples of $Cs_{0.3}V_2O_5$, CsV_2O_5, and $Cs_2V_5O_{13}$ and of adjacent compositions were prepared under similar formation conditions.

Crystals of $Cs_{0.3}V_2O_5$, CsV_2O_5, $Cs_2V_2O_{13}$, and $Cs_xV_3O_7$ were grown from fused mixtures of $CsVO_3$ and V_2O_5 in controlled atmospheres in a minifurnace which permitted continuous visual observation through a stereomicroscope. The charges, typically weighing some 200 mg, were contained in 1-ml Pt crucibles. The minifurnace and the method of growth and separation of crystals from the melt have been previously described (*13*).

To generate oxygen partial pressures in the range $1–10^{-4}$ atm, controlled flows of oxygen and argon were mixed. Lower oxygen partial pressures were obtained from dehydrated mixtures of CO and CO_2. In order to stabilize the oxygen fugacity the CO/CO_2 gas mixture was passed over a Ni/NiO solid buffer, kept at a specific temperature (400–600°C) in a separate furnace, prior to entering the sample space in the minifurnace. The oxygen activity in the dynamic atmosphere in contact with the sample was monitored by means of an yttria-stabilized zirconia solid electrolyte emf cell.

The CsV_2O_5 crystals, brownish platelets with typical dimensions $4 \times 2 \times 0.2$ mm, were grown at $p_{O_2} \approx 10^{-15}$ atm in the temperature range 650–700°C, from melts with $0.33 < x_{Cs_2O} < 0.5$, where $x_{Cs_2O} = n_{Cs_2O}/(n_{Cs_2O} + n_{V_2O_5} + n_{V_2O_3})$.

The $Cs_2V_5O_{13}$ crystals are also formed as thin reddish platelets of typical size $4 \times 3 \times 0.1$ mm. They were grown at $p_{O_2} \approx 10^{-19}$ atm and $T \approx 600$°C from melts with $0.25 < x_{Cs_2O} < 0.35$.

The $Cs_{0.3}V_2O_5$ crystals form thin black prisms and needles, 5 mm in length and at most some 0.2 mm in diameter. They were grown at $p_{O_2} \approx 10^{-4}$ atm and $T \approx 600$°C in the x_{Cs_2O} range 0.1–0.3.

$Cs_xV_3O_7$ crystals form black prisms ($5 \times 0.5 \times 0.3$ mm) and were grown from melts with $0.1 < x_{Cs_2O} < 0.2$ at $T \approx 650$°C and $p_{O_2} \approx 10^{-16}$ atm. In particular, the crystal with the composition $Cs_{0.33}V_3O_7$, characterized by different methods and discussed in the following sections, was grown at $p_{O_2} = 6.0 \times 10^{-17}$ atm from a minute solid residue (the seed) in a melt with $x_{Cs_2O} = 0.115$. After a temperature decrease from 638 to 630°C during 4 hr the crystal ($4 \times 0.3 \times 0.3$ mm) was separated from the liquid.

Microprobe Analysis

The Cs content of the $Cs_xV_2O_5$ and $Cs_xV_3O_7$ crystals, used in the conductivity measurements and in the precise lattice parameter determinations described below, was determined by means of microprobe analysis in a scanning electron microscope (JEOL JSM U-3) connected to an energy dispersive spectrometer (LINK Ltd., 860-S2). Cs_2SO_4, VO_2, and the stoichiometric

compound $Cs_2V_5O_{13}$ were used as standards. Five different areas of each crystal were analyzed, and the Cs and V content was found to be constant to within ±0.5 w% in each crystal.

X-Ray Diffraction Studies

The previous estimate of the upper composition limit for $Cs_xV_3O_7$ ($x = 0.4$) was primarily based on crystallographic considerations (*7*). In order to correlate the Cs content of this phase with unit cell dimensions, a series of powder samples on the composition line $Cs_xV_3O_7$ and close to this line have been prepared. The samples were characterized by means of their X-ray powder patterns, recorded at room temperature in a Guinier–Hägg focusing camera, using Cu$K\alpha_1$ radiation and with KCl as internal standard. The patterns were evaluated in a single-beam microdensitometer specially designed for X-ray powder diffraction photographs (*14*).

Samples of the composition $Cs_xV_3O_7$ with $0.30 \lesssim x \lesssim 0.40$ were almost monophasic. Thus only traces of one or a few extra lines could be detected, and these could be assigned to impurities such as VO_2, V_6O_{13}, $Cs_{0.3}V_2O_5$, and $Cs_2V_5O_{13}$. No trace of $Cs_xV_3O_7$ could be detected in photographs of samples with $x < 0.25$.

With increasing Cs content the *c*-axis increases and the *a*-axis decreases as shown in Figs. 1a and b. The unit cell volume (also indicated in Fig. 1b) is found to be smaller at higher x values.

It was observed that when samples with a total composition off the $Cs_xV_3O_7$ line contained a Cs-rich impurity phase such as $Cs_2V_5O_{13}$, and when the amount of this phase decreased after a second annealing period, an increase in the *c*-axis and a decrease in the *a*-axis of $Cs_xV_3O_7$ occurred, as expected for a transfer of Cs from $Cs_2V_5O_{13}$ to $Cs_xV_3O_7$. In the case of a Cs-poor impurity phase such as VO_2 or V_6O_{13}, the reverse changes in the lengths of the axes were noted. These observations seem to support the trend visualized in Figs. 1a and b.

In conclusion, this study indicates a compositional range $0.30 \lesssim x \lesssim 0.40$ for $Cs_xV_3O_7$ at 470°C, with the maximum and minimum values of the lattice parameters as indicated in Figs. 1a and b.

The X-ray powder patterns of samples containing $Cs_{0.3}V_2O_5$ did not reveal any systematic variation of the hexagonal cell parameters of this phase with the weighed-in

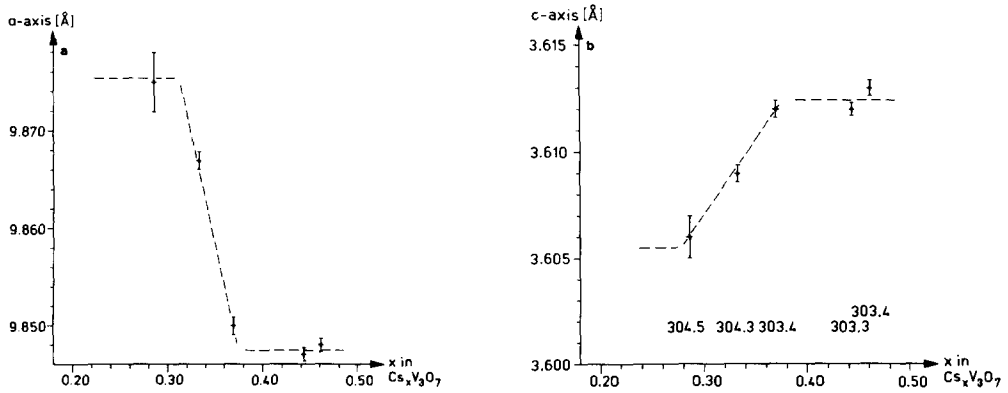

FIG. 1. Variations in unit cell dimensions of $Cs_xV_3O_7$ with weighed-in composition (x) of samples annealed at 470°C for 4 weeks. (a) *a*-axis, (b) *c*-axis. The numbers below the *c*-axis graph are cell volumes in Å^3.

composition. Neither in this case could pure monophasic powder samples be prepared. The cell parameters did, however, vary from sample to sample with the a-axis ranging from 14.377 ± 6 to 14.346 ± 3 Å and the c-axis from 3.611 ± 2 to 3.605 ± 2 Å, with no obvious correlation of a and c.

An analysis of the X-ray powder patterns of CsV_2O_5 and $Cs_2V_5O_{13}$ and samples around these compositions showed that CsV_2O_5 (a = 7.026(5) Å, b = 9.897(2) Å, c = 7.787(3) Å, β = 90.67(3)°) and $Cs_2V_5O_{13}$ (a = 7.765(2) Å, c = 11.747(2) Å) were stoichiometric compounds. Weak extra lines, which could be assigned to impurity compounds, appeared in all photographs of the formally stoichiometric samples.

The difficulties encountered in producing monophasic powder samples, in spite of extended annealing periods with remixing, were probably due to insufficient homogenization in combination with slow reaction rates at the comparatively low preparation temperatures used. At higher preparation temperatures a liquid phase will form, which complicates the reaction paths as discussed in Ref. (*12*).

Precision determinations of the $Cs_xV_3O_7$ lattice parameters have been performed by the Bond method (*15*) on a single crystal (4 × 0.3 × 0.3 mm) with the composition $Cs_{0.33}V_3O_7$. The purpose was to elucidate whether the anomalies observed in the electrical conductivity graphs of $Cs_xV_3O_7$ crystals (see below) have any counterpart in the variation of the lattice parameters with temperature.

In the present study a specially constructed Bond-type diffractometer (*16*) was used with Cu$K\alpha_1$ radiation (λ = 1.540562 Å). The accuracy of the method is strongly dependent on the experimental conditions. In order to obtain good resolution of the $K\alpha$ doublets and high precision, the 7 5 0 and 0 0 4 reflexions were selected for the lattice parameter determinations. This made it possible to determine the unit cell dimensions with an accuracy of 0.001 Å. The temperature interval studied was 125–300 K, and the temperature was kept constant to within ±0.05 K with an electronically controlled thermostat (*16*).

The lattice parameters a and c are plotted versus T in Fig. 2. For $T \lesssim 250$ K the c-axis is almost constant. Around 255 K there is a small decrease followed by a slight linear increase with increasing temperature. The variation in the a-axis is much more pronounced. For $125 \lesssim T \lesssim 220$ K this axis increases linearly with the temperature, with $da/dT = 0.78 \times 10^{-4}$ Å/K. In the temperature interval $230 \lesssim T \lesssim 255$ K a larger da/dT value is observed (1.03×10^{-4} Å/K) while for $255 \lesssim T \lesssim 265$ K the a-axis is almost constant, and then increases linearly with $da/dT = 0.89 \times 10^{-4}$ Å/K. The cell parameter/temperature graphs will be further discussed (vide infra).

Magnetic Susceptibility Measurements

The magnetic susceptibilities of the four mixed-valence Cs–V oxides were measured according to the Faraday method. As strictly monophasic powder samples could not be prepared, crushed single crystals, grown as described above, were used. Typically, samples of 5–10 mg were used. Data were collected with increasing temperature

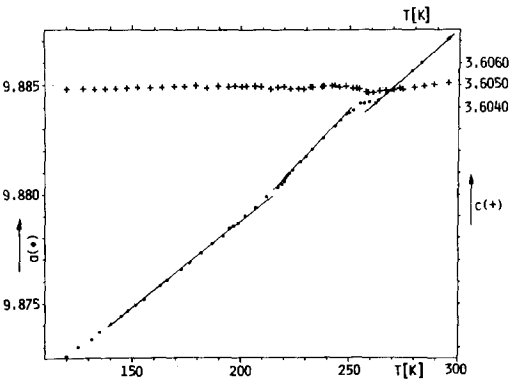

FIG. 2. Variation with temperature in unit cell dimensions of a single crystal of $Cs_{0.33}V_3O_7$.

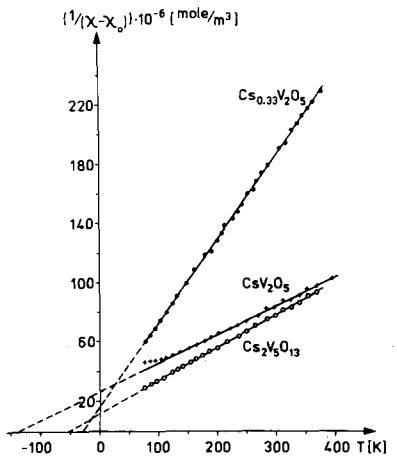

FIG. 3. Plots of the reciprocal paramagnetic susceptibilities vs temperature of three cesium vanadium (IV, V) oxides (crushed single crystals). χ_0 is the temperature-independent contribution to the susceptibility, subtracted from the measured value χ.

from 77 to 400 K in a He atmosphere and $HgCo(SCN)_4$ was used as standard (*17*). The apparatus is described elsewhere (*18*).

The results obtained for $Cs_2V_5O_{13}$, CsV_2O_5, and $Cs_{0.3}V_2O_5$ are plotted in Fig. 3. It is seen that Curie–Weiss' law

$$\chi = \frac{C}{T-\theta} + \chi_0$$

is generally obeyed.

The molar effective magnetic moments, p_{eff}, Weiss' constants, θ, and the χ_0 values for the various compounds were obtained from nonlinear least-squares refinements based on the experimental data. In Fig. 3 the $(\chi - \chi_0)^{-1}$ values are plotted versus temperature.

χ_0 thus originates from the diamagnetism of the electron core and a temperature-independent paramagnetic contribution.

The following parameters were found for $Cs_2V_5O_{13}$: $\chi_0 = 2.91 \times 10^{-9}$ m³/mole, $\theta = -55$ K and $p_{eff} = 1.69$. This p_{eff} value is consistent with the structure, which suggests four V^{5+} for each V^{4+} (see below).

The $Cs_xV_2O_5$ crystals used for the magnetic susceptibility measurements were grown from Cs-rich melts, giving x values close to 0.33 according to the microprobe analysis. The observed p_{eff} value, 1.83/g-atom Cs, is consistent with one V^{4+} per CsV_6O_{15} unit. The calculations yielded a θ value of -30 K and $\chi_0 = 1.15 \times 10^{-9}$ m³/mole. Lukács *et al.* (*19*) reported a p_{eff} value of 1.73 for polycrystalline CsV_6O_{15} from a single measurement at 300 K.

In the high-temperature region Curie–Weiss' behavior is also observed for CsV_2O_5: $\chi_0 = 4.34 \times 10^{-10}$ m³/mole and $p_{eff} = 1.84$. The latter value suggests the occurrence of one unpaired electron/formula unit. Below $T = 120$ K χ shows a deviation from Curie–Weiss' law, however, This observation and the relatively large θ value obtained (-140 K) may indicate an antiferromagnetic coupling at lower temepratures.

The $Cs_xV_3O_7$ crystals used in the magnetic susceptibility measurements were grown under the same conditions as those described above for $Cs_{0.33}V_3O_7$. This compound exhibits a typical antiferromagnetic behavior with a Néel temperature of ≈230 K, as seen in Fig. 4. In the high-temperature limit, temperature-dependent paramagnetism is observed with a p_{eff} value close to the "spin-only" value of 1.73/V^{4+} ion at 300 K.

Electrical Conductivity Measurements

The crystals for the conductivity mea-

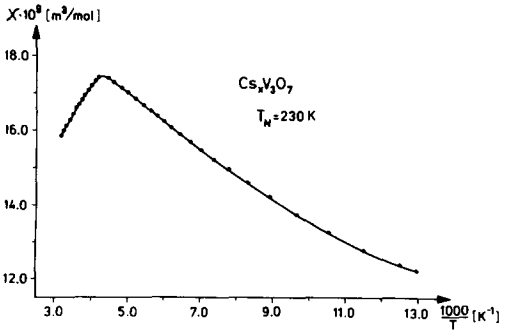

FIG. 4. The $\chi = f(T^{-1})$ plot for $Cs_xV_3O_7$ (crushed single crystals).

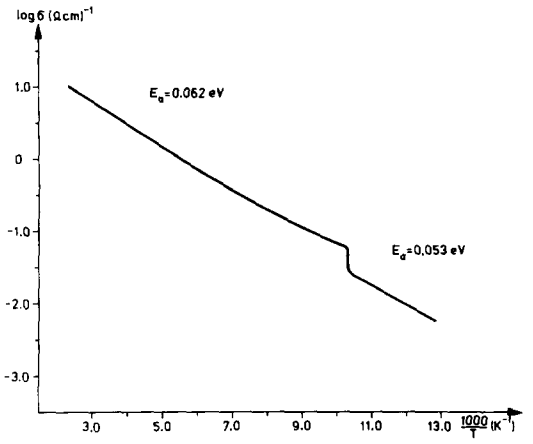

FIG. 5. The log $\sigma = f(T^{-1})$ plot for a crystal of $Cs_{0.31}V_2O_5$ (measurement parallel to the c-axis).

surements were from 0.5 to 4.0 mm in length. The standard four-probe arrangement was used, with contacts applied onto the crystals as described by Hörlin *et al.* (*20*). This setup allows resistances ranging from 10^7 to 10^{-3} Ω to be recorded. The measurements were performed in the temperature interval 80–400 K, with heating and cooling rates of 0.01T/min. Data were recorded both during heating and cooling. Due to the uncertainty in the cross section in the somewhat irregulary shaped crystals, the error in the absolute value of the conductivity is estimated to be 15–20%.

CsV_2O_5 and $Cs_2V_5O_{13}$ both are insulators with resistivities exceeding 10^5 Ω cm around room temperature.

The hexagonal $Cs_xV_2O_5$ phase exhibits semiconducting properties. In a crystal with $x = 0.31$ a semiconductor → semiconductor transition was found to occur at 97 K (see Fig. 5). The activation energy; E_a = 0.053 eV in the low-temperature region (T < 97 K) is smaller than that for $T \gtrsim 150$ K (E_a = 0.062 eV). In the temperature interval $97 < T \lesssim 150$ K a nonlinear relation between log σ and T^{-1} is observed. This behavior may indicate a variation of the band gap with temperature.

The same type of curve is observed with crystals of slightly different Cs content. Crystals grown from Cs-rich melts were found to have slightly higher Cs content and the S.C. → S.C. transition temperature seems to shift a few degrees toward higher temperatures with Cs content increasing from $x = 0.30$ to $x = 0.33$.

The log $\sigma = f(T^{-1})$ graphs for $Cs_xV_3O_7$ with $x = 0.30$ and $x = 0.33$ are given in Fig. 6. In the high-temperature range ($T > 265$ K) semiconducting behavior is observed, with $E_a = 0.042$ eV. In the antiferromagnetic low-temperature region ($T \lesssim 150$ K) both compositions exhibit semiconducting properties, with a S.C. → S.C. transition at 98 and 115 K for $x = 0.30$ and 0.33, respectively. The transition temperature thus increases with increasing Cs content. An E_a value of 0.056 eV is found both above and below this temperature. We have also observed that for $x > 0.33$ the low-temperature part of the log σ versus T^{-1} graph tends to be nonlinear.

The shape of the log σ versus T^{-1} graph in the temperature range comprising the transition from the low-temperature antiferromagnetic state (with E_a = 0.056 eV) to the high-temperature paramagnetic state (E_a = 0.042 eV) also varies with the Cs content.

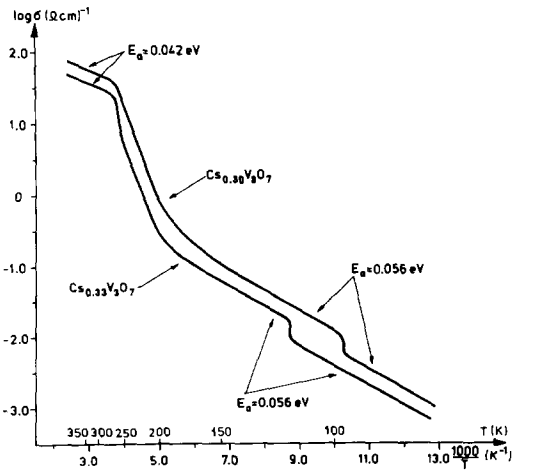

FIG. 6. The log $\sigma = f(T^{-1})$ plot for two crystals of $Cs_xV_3O_7$ with different compositions.

The $Cs_{0.30}V_3O_7$ graph is nonlinear from $T \approx$ 150 K and almost linear above T = 265 K. The latter temperature is taken as the onset temperature of the paramagnetic state. For $Cs_{0.33}V_3O_7$, the nonlinear portion of the graph extends over a more limited temperature range, and the linear increase in log σ with T^{-1} occurs in two steps, one ended at $T \approx$ 255 K and the other at T = 265 K as seen in Fig. 6. For crystals with higher Cs contents, the stepwise character of the transition from the antiferromagnetic to the paramagnetic state is even more pronounced.

The conductivity of the $Cs_{0.33}V_3O_7$ crystal was measured both parallel and normal to the c-axis. No significant anisotropy was detectable, nor did the shapes of the two log σ versus T^{-1} graphs differ significantly.

Structural Considerations

The structure of CsV_2O_5 (*10*) is built up of layers formed by pairs of edge-sharing VO_5 square pyramids and bridging VO_4 tetrahedra. The layers are held together by Cs^+ ions. One layer of V–O polyhedra is illustrated in Fig. 7. The bond distances suggest that the cationic charges are segregated: V^{5+} is located in the tetrahedra and V^{4+} in the square pyramids. The location of charges on different crystallographic sites is consistent with the observed high electrical resistivity and the Curie–Weiss' law behavior (p_{eff} = 1.83/V^{4+}).

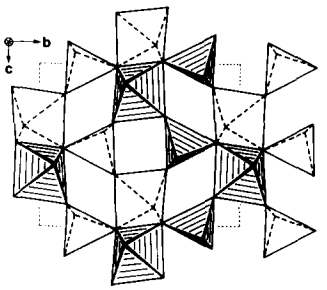

FIG. 7. One layer of V–O polyhedra in CsV_2O_5 (monoclinc). The Cs^+ sites between the layers are not indicated.

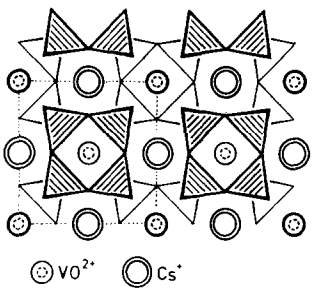

FIG. 8. The structure of $Cs_2V_5O_{13}$ (tetragonal).

The structure of $Cs_2V_5O_{13}$ (*9*), illustrated in Fig. 8, can be described as built up of $V_4O_{12}^{4-}$ ions, consisting of isocyclic four-membered rings of VO_4 tetrahedra. These units are linked by vanadyl (VO^{2+}) and Cs^+ ions. The observed insulating properties and the Curie–Weiss' law behavior of $Cs_2V_5O_{13}$ indicate the V^{4+} state to be localized. These observations are in agreement with the previous analysis of the structural details (*9*), suggesting that the V^{5+} ions are to be found in the VO_4 tetrahedra while the V^{4+} state is associated with the vanadyl ions.

A structural study of $Cs_xV_2O_5$ (*8*) has shown that two crystallographically different types of V atoms, both located in VO_5 square pyramids are present in the structure. The VO_5 pyramids are linked together by edge-sharing and corner-sharing so as to form two types of tunnels, as seen in Fig. 9.

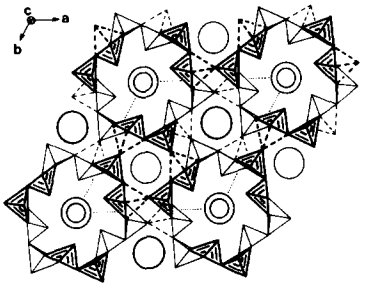

FIG. 9. The hexagonal substructure of $Cs_xV_2O_5$. The rings indicate Cs^+ sites.

The Cs^+ ions reside in these tunnels. According to the crystal structure refinement, approximately $\frac{2}{3}$ of the total Cs content is distributed in the tunnels at the crystallographic site $x = \frac{1}{3}$, $y = \frac{2}{3}$, and $z = \frac{1}{4}$. The remaining Cs^+ ions are located in the tunnels at $x = y = 0$.

Crystals annealed at 470°C for 1 month gave rise to superstructure reflexions, which could be ascribed to an ordering of the Cs^+ ions in the tunnels at $x = y = 0$ (*8*). A similar type of ordering is, however, less likely in the present case, since the crystals were not annealed. The partial occupancy of the Cs^+ ion sites in the tunnels suggests that x in $Cs_xV_2O_5$ may vary. However, the X-ray analysis of powder samples, and the microprobe analysis of crystals grown from melts with various Cs/V ratios, have shown that if a compositional range does exist it must be very narrow, with x varying at most between 0.30 and 0.33.

The main difference between the two types of vanadium in square pyramids is that one of them coordinates a sixth, rather remote oxygen, formally completing a distorted octahedron, as illustrated in Fig. 9. The electrical and magnetic properties of $Cs_xV_2O_5$ suggest that the electron associated with the V^{4+} ion is localized. However, considering that only one V^{4+} ion per CsV_6O_{15} unit is present, it is not possible from structural considerations to ascribe the V^{4+} ions definitely to one of the two crystallographically different vanadium sites.

In the absence of structural information in the low-temperature region, it is not possible to draw any conclusions about the nature of the S.C.-to-S.C. transition at 97 K. It is, however, notable that the activation energy for conduction is larger in the high-temperature than in the low-temperature region and that the magnetic susceptibility curve exhibits no anomaly around 97 K.

The structure of $Cs_xV_3O_7$ (*7*) resembles that of $Cs_xV_2O_5$ to a great extent, as seen in Fig. 10. However, in $Cs_xV_3O_7$ only one type of VO_5 square pyramid and one type of Cs-containing tunnel are present. The X-ray analysis of powder samples indicates a compositional range of $0.30 \lesssim x \lesssim 0.40$, as discussed above. The upper limit corresponds to the maximum occupancy of the tunnels (*7*).

Above 265 K, $Cs_{0.33}V_3O_7$ exhibits temperature-dependent paramagnetism and semiconducting properties, indicating a localized V^{4+} state. There is no clear structural evidence for a segregation of V^{4+} and V^{5+} ions onto different crystallographic sites. The mean V–O distance in the VO_5 pyramid is, however, slightly longer than expected for such a polyhedron containing only V^{5+} ions. This indicates a statistical distribution of the V^{4+} and V^{5+} ions over the V sites.

The antiferromagnetic behavior of $Cs_{0.33}V_3O_7$ in the low-temperature region suggests that the V^{4+} ions are ordered rather than statistically distributed. The absence of discrete changes in the lattice parameters in the temperature range 125–300 K (Fig. 2) indicates that the transition from the paramagnetic to the antiferromagnetic state is not accompanied by any major structural changes.

One single crystal of the composition $Cs_{0.33}V_3O_7$ (according to the microprobe analysis) was subjected to both precision measurements of the lattice dimensions and

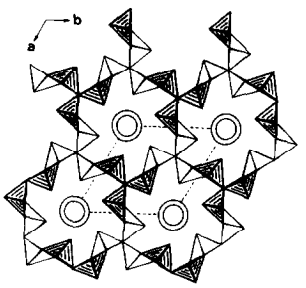

FIG. 10. The hexagonal substructure of $Cs_xV_3O_7$. The rings indicate Cs^+ sites.

conductivity measurements. Log σ shows a tendency to change stepwise with T^{-1} when the crystal passes from the antiferromagnetic to the paramagnetic state (see Fig. 6). Small but reproducible changes of da/dT in the plot of the a-axis length versus T (Fig. 2) were detected at the temperatures of the stepwise change in the log $\sigma = f(T^{-1})$ graph. In the absence of detailed structural information on the antiferromagnetic state it is not possible to decide whether this behavior might be explained by an order–disorder process.

From electrical conductivity measurements on single crystals of the monoclinic tunnel structure β-$Na_xV_2O_5$, both parallel and normal to the b-axis, a large anisotropy ($\sigma_\parallel/\sigma_\perp$ = 130–400) was discovered (*21*). This fact, as well as results of optical (*22*) and EPR studies (*5*), support the view that β-$Na_xV_2O_5$ is a quasi-one-dimensional conductor. The structure of β-$Na_xV_2O_5$ exhibits great differences in the V–O distances ($(V–O)_{max}$ = 2.34 Å, $(V–O)_{min}$ = 1.56 Å). This reflects a segmentation of the structure, which forces the electrons to discriminate among conduction paths. In the structure of $Cs_xV_3O_7$, the V–O distances do not differ appreciably: 1.898, 1.902, 1.953, and 1.572 Å (the last one between vanadium and the apex oxygen of the pyramid, pointing into the tunnel). Hence, anisotropy in the electrical conductivity is not expected on crystallographic grounds, nor is it observed.

Acknowledgments

The authors wish to express their sincere thanks to Professor Lars Kihlborg and Dr. Karl-Axel Wilhelmi for their constructive criticism of this work. We are also indebted to Mr. Tomasz Niklewski, who performed the microprobe analyses, Dr. Damian Kucharczyk, who took part in the Bond-diffractometer measurements, and to Dr. Sven Westman, who corrected the English of the manuscript. This work has been sponsored by the Swedish Natural Science Research Council.

References

1. H. Flood and H. Sørum, *Tidsskr. Kjemi Bergves. Metall.* **3,** 55 (1943).
2. H. Flood, Th. Krog, and H. Sørum, *Tidsskr. Kjemi Bergves. Metall.* **6,** 59 (1946).
3. P. Hagenmuller, *in* "Comprehensive Inorganic Chemistry" (Trotman-Dickenson, Ed.), Vol. 4, p. 569, Pergamon, Elmsford, N.Y. (1973).
4. P. Hagenmuller, *in* "Crystal Structure and Bonding in Inorganic Chemistry" (Rooymans and Rabenau, Eds.), North-Holland/Elsevier, Amsterdam (1975).
5. A. Friederich, D. Kaplan, N. Sol, and R. H. Wallis, *J. Phys. Lett.* **39**(19), 343 (1978).
6. B. Forslund, *Chem. Scr.*, in press.
7. K. Waltersson and B. Forslund, *Acta Crystallogr. Sect. B* **33,** 775 (1977).
8. K. Waltersson and B. Forslund, *Acta Crystallogr. Sect. B* **33,** 780 (1977).
9. K. Waltersson and B. Forslund, *Acta Crystallogr. Sect. B* **33,** 784 (1977).
10. K. Waltersson and B. Forslund, *Acta Crystallogr. Sect. B* **33,** 789 (1977).
11. B. Forslund, *Chem. Scr.*, in press.
12. B. Forslund, *Chem. Scr.*, in press.
13. B. Forslund and B. Jelinski, *Mater. Res. Bull.*, in press.
14. K.-E. Johansson, T. Palm, and P.-E. Werner, *J. Phys. E* **13,** 1289 (1980).
15. W. L. Bond, *Acta Crystallogr.* **13,** 814 (1960).
16. K. Łukaszewicz, D. Kucharaczyk, M. Malinowski, and A. Pietraszko, *Krist. Tech.* **13,** 561 (1978).
17. S. A. Kizhaev, P. V. Usachev, and V. M. Yudin, *Fiz. Tverd. Tela* **13,** 2829 (1971).
18. T. Hörlin and B. Blom, *Chem. Commun. Univ. Stockholm,* 5 (1977).
19. I. Lukács, C. Strusievici, and C. Liteanu, *Rev. Roum. Chim.* **16,** 245 (1971).
20. T. Hörlin, T. Niklewski, and M. Nygren, *Chem. Scr.* **13**(5), 201 (1978–79).
21. R. H. Wallis, N. Sol, and Z. Zylbersztejn, *Solid State Commun.* **23**(8), 539 (1977).
22. D. Kaplan and A. Zylbersztejn, *J. Phys. (Paris) Lett.* **37**(5), 123 (1976).